NASA/TM—2010-216222 IFASD–2009–101

# Harmonic Balance Computations of Fan Aeroelastic Stability

*Milind A. Bakhle*
*Glenn Research Center, Cleveland, Ohio*

*T.S.R. Reddy*
*University of Toledo, Toledo, Ohio*

August 2010

# NASA STI Program . . . in Profile

Since its founding, NASA has been dedicated to the advancement of aeronautics and space science. The NASA Scientific and Technical Information (STI) program plays a key part in helping NASA maintain this important role.

The NASA STI Program operates under the auspices of the Agency Chief Information Officer. It collects, organizes, provides for archiving, and disseminates NASA's STI. The NASA STI program provides access to the NASA Aeronautics and Space Database and its public interface, the NASA Technical Reports Server, thus providing one of the largest collections of aeronautical and space science STI in the world. Results are published in both non-NASA channels and by NASA in the NASA STI Report Series, which includes the following report types:

- TECHNICAL PUBLICATION. Reports of completed research or a major significant phase of research that present the results of NASA programs and include extensive data or theoretical analysis. Includes compilations of significant scientific and technical data and information deemed to be of continuing reference value. NASA counterpart of peer-reviewed formal professional papers but has less stringent limitations on manuscript length and extent of graphic presentations.

- TECHNICAL MEMORANDUM. Scientific and technical findings that are preliminary or of specialized interest, e.g., quick release reports, working papers, and bibliographies that contain minimal annotation. Does not contain extensive analysis.

- CONTRACTOR REPORT. Scientific and technical findings by NASA-sponsored contractors and grantees.

- CONFERENCE PUBLICATION. Collected papers from scientific and technical conferences, symposia, seminars, or other meetings sponsored or cosponsored by NASA.

- SPECIAL PUBLICATION. Scientific, technical, or historical information from NASA programs, projects, and missions, often concerned with subjects having substantial public interest.

- TECHNICAL TRANSLATION. English-language translations of foreign scientific and technical material pertinent to NASA's mission.

Specialized services also include creating custom thesauri, building customized databases, organizing and publishing research results.

For more information about the NASA STI program, see the following:

- Access the NASA STI program home page at *http://www.sti.nasa.gov*

- E-mail your question via the Internet to *help@sti.nasa.gov*

- Fax your question to the NASA STI Help Desk at 443–757–5803

- Telephone the NASA STI Help Desk at 443–757–5802

- Write to:
  NASA Center for AeroSpace Information (CASI)
  7115 Standard Drive
  Hanover, MD 21076–1320

NASA/TM—2010-216222 IFASD–2009–101

# Harmonic Balance Computations of Fan Aeroelastic Stability

*Milind A. Bakhle*
*Glenn Research Center, Cleveland, Ohio*

*T.S.R. Reddy*
*University of Toledo, Toledo, Ohio*

Prepared for the
International Forum on Aeroelasticity and Structural Dynamics (IFASD 2009)
cosponsored by CEAS and AIAA
Seattle, Washington, June 21–25, 2009

National Aeronautics and
Space Administration

Glenn Research Center
Cleveland, Ohio 44135

August 2010

## Acknowledgments

Support for this work from the NASA Fundamental Aeronautics Program is gratefully acknowledged. The authors would like to thank Dr. Nateri Madavan and Dr. James Heidmann (Associate Principal Investigators for the Subsonic Fixed Wing Project) for their support of this work. The authors would also like to thank Mr. Brian Fite for providing us the opportunity to work with this configuration. The authors would like to acknowledge Dr. Jeffrey Thomas of Duke University for his support of this work.

This work was sponsored by the Fundamental Aeronautics Program
at the NASA Glenn Research Center.

*Level of Review*: This material has been technically reviewed by technical management.

Available from

NASA Center for Aerospace Information
7115 Standard Drive
Hanover, MD 21076–1320

National Technical Information Service
5301 Shawnee Road
Alexandria, VA 22312

Available electronically at http://gltrs.grc.nasa.gov

# Harmonic Balance Computations of Fan Aeroelastic Stability

Milind A. Bakhle
National Aeronautics and Space Administration
Glenn Research Center
Cleveland, Ohio 44135

T.S.R. Reddy
University of Toledo
Toledo, Ohio 43606

## Abstract

A harmonic balance (HB) aeroelastic analysis, which has been recently developed, was used to determine the aeroelastic stability (flutter) characteristics of an experimental fan. To assess the numerical accuracy of this HB aeroelastic analysis, a time-domain aeroelastic analysis was also used to determine the aeroelastic stability characteristics of the same fan. Both of these three-dimensional analysis codes model the unsteady flowfield due to blade vibrations using the Reynolds-averaged Navier-Stokes (RANS) equations. In the HB analysis, the unsteady flow equations are converted to a HB form and solved using a pseudo-time marching method. In the time-domain analysis, the unsteady flow equations are solved using an implicit time-marching approach. Steady and unsteady computations for two vibration modes were carried out at two rotational speeds: 100 percent (design) and 70 percent (part-speed). The steady and unsteady results obtained from the two analysis methods compare well, thus verifying the recently developed HB aeroelastic analysis. Based on the results, the experimental fan was found to have no aeroelastic instability (flutter) at the conditions examined in this study.

## 1.0 Introduction

Aircraft engine fan and compressor blades are susceptible to flutter, which can lead to catastrophic failure. Flutter problems will likely be encountered more often in newer engine designs that are being developed to reduce noise, improve performance, and reduce weight—using thinner blades, more complex blade geometry, and higher blade loading. To avoid unexpected flutter during engine development and testing, it is important to develop and validate numerical tools that can be used to verify aeroelastic stability using high-fidelity physics-based models. Research has been on-going in the development, validation and application of high fidelity models for aeroelastic vibrations in aircraft engine fan, compressor and turbine blades (Ref. 1). Recent work has included time-domain solution of the Reynolds-averaged Navier-Stokes (RANS) equations to provide the unsteady flowfield and unsteady aerodynamic loads on vibrating blades. An example of such work is the TURBO aeroelastic analysis code (Refs. 2 and 3), which has predicted aeroelastic stability characteristics that agreed well with experimental data. However, such time-domain solutions require large computational times due to the long startup transients that must decay before solutions become periodic. To reduce computational cost while maintaining the same level of prediction accuracy, the harmonic balance (HB) method has recently been developed and used (Ref. 4). In this approach, each flow variable is represented by a Fourier series in time, leading to a HB form of the RANS equations. The resulting equations can be solved using methods that are typically used for steady flow problems such as pseudo-time marching and local time stepping. The HB approach may thus provide a high fidelity modeling capability with a reduced computational cost compared to the typical time-domain solution method.

In the present study, the aeroelastic stability (flutter) characteristics of an experimental fan are analyzed using a HB RANS aeroelastic analysis and computer code developed by Hall et al. (Refs. 4 and 5). Since the focus here is to verify the recently developed HB aeroelastic code by direct comparison, a time-domain RANS aeroelastic code (Ref. 2) (TURBO) is also used to analyze the same experimental

fan. The objective is to validate the accurate computation of unsteady aerodynamics due to vibrating blades. The experimental fan configuration used in this study is described in detail in Reference 6. This fan was designed to demonstrate a noise-reduction technology based on trailing edge flow injection. Note, however, that in this paper, the fan is analyzed only in the mode of operation with no trailing edge flow injection.

Both analyses used in this study solve the three-dimensional unsteady, RANS equations with the ability to model a rotating blade row with harmonic blade vibrations or incoming periodic distortions. For flutter calculations, the blade vibration is prescribed to be the modal deflection and a frequency, both of which are calculated from a separate structural dynamics analysis. Computations are performed in a single blade passage for both steady and unsteady analyses. In the HB analysis (Refs. 4 and 5), the resulting unsteady pressures on the blade are used to calculate a generalized aerodynamic force and then an eigenvalue problem is solved to calculate the aerodynamic damping. The damping value is needed to determine the aeroelastic stability in the selected vibration mode and traveling wave pattern (Ref. 7). In the time-domain analysis (Ref. 2), the unsteady pressures are used to calculate a work-per-cycle that is then used to calculate the aerodynamic damping, which is then used to determine aeroelastic stability. This paper describes the aeroelastic stability calculations and compares the results from the HB and time-domain analyses. Results are presented at design speed and part-speed for aeroelastic analysis with the first and second vibration modes, followed by conclusions.

# 2.0 Analyses Methods

## 2.1 Aeroelastic Model

The equations of motion for a fan blade (with all blades assumed to be identical) can be written as

$$[M]\{\ddot{q}\}+[K]\{q\}=[A]\{q\} \tag{1}$$

where $[M]$ and $[K]$ are generalized mass and stiffness matrices, $\{q\}$ is the generalized displacement vector, and $[A]$ is the blade vibration-dependent generalized aerodynamic force matrix. The matrices $[M]$, $[K]$, and $[A]$ are of size $nm \times nm$; $\{q\}$ is of size $nm \times 1$; $nm$ is the number of modes.

The elements of $[M]$ and $[K]$ are obtained from a free-vibration analysis using commercial structural dynamics analysis software. The matrices $[M]$ and $[K]$ are diagonal and their non-zero elements are related as

$$K_i = M_i \omega_i^2 (1 + 2i\zeta) \tag{2}$$

where $\omega_i$ is the natural frequency of the $i^{\text{th}}$ mode, and $\zeta$ is the structural damping ratio; usually the mode shapes are mass-normalized and therefore $M_i = 1$.

Since all the blades are identical (that is, a tuned rotor), the aeroelastic modes consist of individual blades vibrating with equal amplitudes at a fixed interblade phase angle between adjacent blades. Hence, the motion of a blade in $r^{\text{th}}$ interblade phase angle mode can be written as

$$\{q\} = \{q_r\} e^{i\omega t} e^{i\sigma_r s} \tag{3}$$

where $\omega$ is the vibration frequency, $\sigma_r$ is the interblade phase angle related to nodal diameter ($ND$) pattern of the traveling wave and number of blades $N_{\text{blades}}$ as

$$\sigma_r = 2\pi\, ND / N_{\text{blades}}, \quad -N_{\text{blades}} / 2 \le ND \le N_{\text{blades}} / 2 \tag{4}$$

Thus, the equations of motion for a blade become

$$-\omega[M]\{q_r\}+[K]\{q_r\}=[A_r]\{q_r\} \tag{5}$$

The following subsections describe the flutter calculation method used with the HB code and separately with the time-domain TURBO code.

## 2.2 Harmonic Balance Flutter Analysis

The HB flutter analysis requires calculation of elements of the generalized aerodynamic force matrix $[A_r]$. Unsteady flowfield computations are carried out for each vibration mode and assumed frequency. For a selected value of interblade phase angle, the HB code is used to calculate the unsteady pressure distribution on the blade surface, which is further used to calculate the (complex-valued) elements of the generalized aerodynamic force matrix $[A_r]$. This calculation is repeated for $N_{\text{blades}}$ interblade phase angles given by Equation (4).

To calculate flutter stability, Equation (5) is written in a standard eigenvalue form as:

$$[[P]-\gamma[Q]]\{q_r\}=\{0\} \tag{6}$$

where $[P]=([K]-[A_r])/\omega_o^2; [Q]=[M]; \gamma=(\omega/\omega_o)^2$ and $\omega_o$ is the assumed frequency used in the calculation of the elements of the aerodynamic force matrix $[A_r]$.

The solution of the above eigenvalue problem results in *nm* complex eigenvalues of the form

$$i(\omega/\omega_o)=i\sqrt{\gamma}=\bar{\mu}\pm i\bar{\nu} \tag{7}$$

The real part of the eigenvalue ($\bar{\mu}$) represents the damping ratio, and the imaginary part ($\bar{\nu}$) represents the damped frequency; flutter occurs if $\bar{\mu}\geq 0$ for any eigenvalue.

In the present work, structural damping is set to zero and therefore damping is referred to as aerodynamic damping. Also, note that $\bar{\mu}$ is opposite in sign to damping.

## 2.3 TURBO Work-Per-Cycle Method

The work-per-cycle approach is used in the TURBO analysis to determine flutter stability. First, the flowfield through the blade row is calculated with no prescribed blade vibration. Starting with this converged steady flowfield, blade vibrations are prescribed in a selected mode, frequency, and nodal diameter pattern or phase angle. After the transients in the flowfield decay, and a periodic flowfield is obtained, the work done on the vibrating blade is calculated for a cycle of blade vibration as follows:

$$W=\oint \int_{\text{surface}} -pdA\cdot(\partial X/\partial t)dt \tag{8}$$

where $p$ is the blade surface pressure, $A$ is the surface area vector, $X$ is the position vector, and $t$ is time. For harmonic vibration, the work-per-cycle of oscillation, can be re-written as

$$W=\oint \int_{\text{surface}} -pdA\cdot\delta q_0\omega\cos(\omega t)dt \tag{9}$$

where δ is the modal displacement vector, $q_0$ is the amplitude of the generalized displacement, and ω is the vibration frequency. The aerodynamic damping ratio ($\zeta$) associated with blade vibration is related to the work-per-cycle ($W$) and the average kinetic energy ($K_E$) of the blade over one cycle of vibration through the following equation from Reference 8

$$\frac{W}{K_E} = -\frac{8\pi\zeta}{\sqrt{1-\zeta^2}} \tag{10}$$

where

$$K_E = \frac{1}{T}\oint \tfrac{1}{2} m V^2 dt \tag{11}$$

$$\zeta = C/C_{cr}\ ; \quad C_{cr} = 2m\omega \tag{12}$$

In the preceding equations, $C$ is the damping, $C_{cr}$ is the critical damping, $m$ is the mass of the blade, $V$ is the surface velocity due to blade vibration, and $T$ is the time period.

For small values of damping ratio which typically occur in aeroelastic calculations of interest, $\zeta << 1$, the aerodynamic damping ratio can be approximated as

$$\zeta \approx -W/8\pi K_E \tag{13}$$

If aerodynamic damping is negative, flutter can occur. Note that the structural damping (material and mechanical damping) has not been considered. Also, note that aerodynamic damping ($\zeta$) is opposite in sign to $\bar{\mu}$.

# 3.0 Results

In this section, results of steady and unsteady computations are presented for an experimental fan described in Reference 6. This fan has 18 blades with a tip diameter of 22 in.; the design parameters are rotational speed of 8750 rpm, pressure ratio of 1.284, tip speed of 840 ft/s, and mass flow rate of 85.7 lbm/s. Steady and unsteady computations were carried out at two rotational speeds: 100 percent (design) and 70 percent (part-speed). The latter rotational speed was selected to investigate, generically, the possibility of part-speed flutter for this fan, with the understanding that multiple speeds must be examined in practice to establish flutter stability of the fan. Unsteady computations were carried out for the first two structural vibration modes (bending and torsion).

Note that in the present work, the HB aeroelastic code was run with very small amplitude vibrations of the fan blade to calculate linearized unsteady aerodynamics for a conventional linear flutter analysis. Also, the amplitude of vibration for the time-domain (TURBO) computations was in a linear range.

## 3.1 Steady Computational Results

The airfoil geometry used in this study was calculated based on static deflections obtained from structural analysis at design speed. The static deflections included the effects of rotational speed and aerodynamic pressure at design condition; nonlinear geometry effects were included in the structural analyses. The same blade geometry was used for both design and part-speed computations. Previous calculations for a different fan (Ref. 2) have shown that changes from the nominal blade geometry due to changes in rotational speed were not significant and therefore a single geometry was used in the present work for computations at both speeds and all operating conditions.

The computational grids used here were generated using commercial software. The grid for the HB computations is shown in Figure 1(a); the grid size is 193 by 33 by 49 for the O-grid block that wraps around the blade airfoil with 193 points around the airfoil, 33 points in the circumferential direction, and 49 points in the spanwise direction. The H-grid blocks in the inlet and exit sections are each 17 by 33 by 49 with 17 points in the streamwise direction, 33 grid points in the circumferential direction, and 49 grid points in the spanwise direction. The tip clearance present in the grid was based on design intent and is modeled using 9 points between the blade tip and casing. For the TURBO time-domain computations, the H-grid, shown in Figure 1(b), has a size of 111 by 41 by 39 with 111 points in the axial direction, 41 points in the spanwise direction, and 39 points in the circumferential direction; 4 cells are used in the tip clearance region.

In the computations, inlet flow conditions consisted of uniform total pressure and total temperature (uniform inflow). The exit flow conditions consisted of a static pressure value prescribed at the hub and calculated at other radial locations using radial equilibrium.

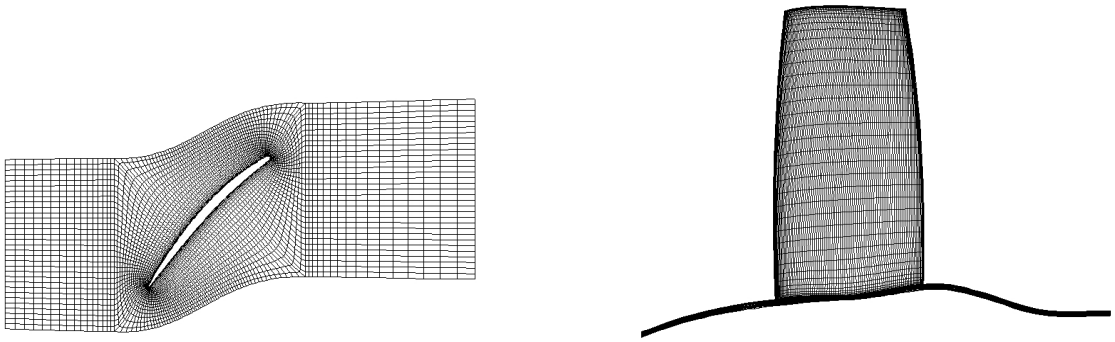


Figure 1(a).—Computational mesh for HB computations.

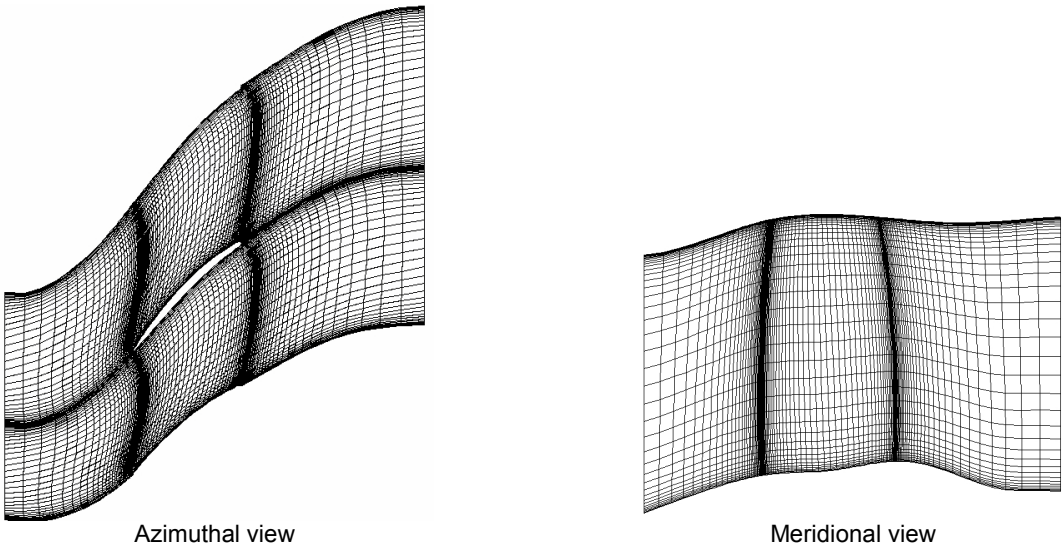


Figure 1(b).—Computational mesh for time-domain TURBO computations.

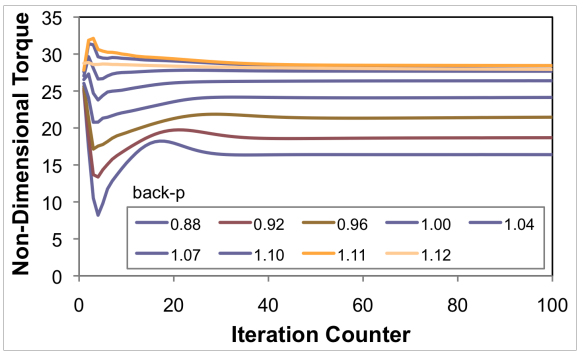


Figure 2.—Steady solution convergence from HB method.

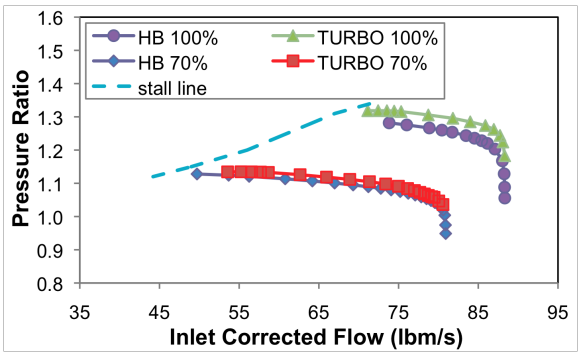


Figure 3.—Fan map showing performance predictions from HB and time-domain codes.

Steady computations were carried out for two rotational speeds (100 and 70 percent). The exit static pressure on the hub was varied to change the mass flow rate and the operating point on the fan map. Thus, two speed lines were generated using each analysis code. Figure 2 shows the convergence of the steady HB computations as a plot of non-dimensional torque with iteration counter (100 iterations per counter). These computations were carried out at 100 percent speed for various values of imposed back-pressure at the exit boundary. As can be noted from Figure 2, excellent convergence was obtained for all operating conditions. Similar convergence was obtained for the computations at 70 percent speed as well as for the computations with the TURBO code at both speeds. All steady results presented here are from well-converged solutions.

The fan map, total pressure ratio versus mass flow rate, is shown in Figure 3 with the results of HB steady computations denoted as HB and the results of the time-domain computations denoted as TURBO. Results are presented for computations at several operating conditions for 100 and 70 percent speeds. The computed results from the two analysis codes correlated well at both speeds. At 100 percent speed, the difference in pressure ratio is <3 percent and the difference is about 1 percent at 70 percent speed. This level of agreement between the two analysis codes is consistent with previous results for another fan configuration as reported in Reference 7. The stall line shown is based on design intent and was not part of the current computations.

Overall, the HB results for pressure ratio show good correlation with the TURBO results, except for a small shift in the speed line towards lower pressure ratio. This shift is slightly larger for 100 percent speed than for 70 percent speed. Also, for both speeds, the HB results show lower mass flow rate than the TURBO results for the same imposed back-pressure although this is not discernable from Figure 3. Figure 4 is a plot of calculated corrected flow rate for various imposed back-pressure values that illustrates the differences in mass flow between TURBO and HB results. The differences between the calculated mass flow rates are not very large, except near the stall line (high back-pressure) at 100 percent speed. Further investigation is required to understand these differences in the results from the two analyses. For the unsteady computations and results to follow, it should be noted that a comparison for the same value of imposed back-pressure would be expected to show differences simply based on the different steady operating conditions that would result from the TURBO and HB analyses.

The efficiency computed from the HB and TURBO computations is plotted in Figure 5 and shows excellent correlation between the two sets of results for both speeds, with some differences near the stall line. It should be noted that significant differences exist between the numerical method used in the TURBO computations and the HB computations. These differences include time-domain versus frequency-domain, numerical discretization, grid, and algorithm used to solve the RANS equations, turbulence modeling, and others. Therefore, the differences in results noted in Figures 3 to 5 are not entirely surprising.

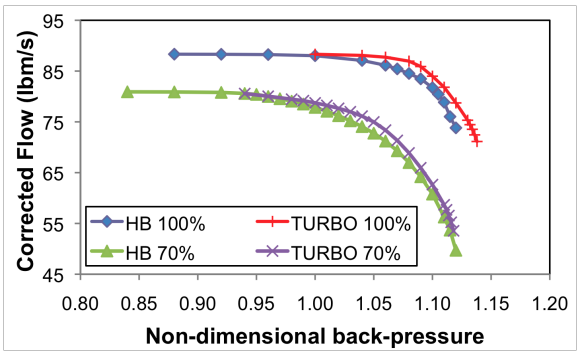


Figure 4.—Variation of mass flow rate with back-pressure from HB and time-domain codes.

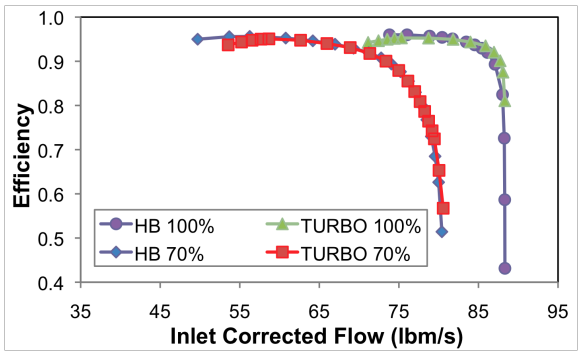


Figure 5.—Predicted efficiency from HB and time-domain codes.

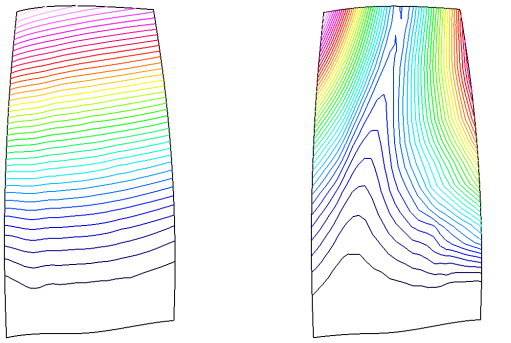

(a) bending, 502 Hz (b) torsion, 1492 Hz

Figure 6.—Un-scaled mode shapes for experimental fan.

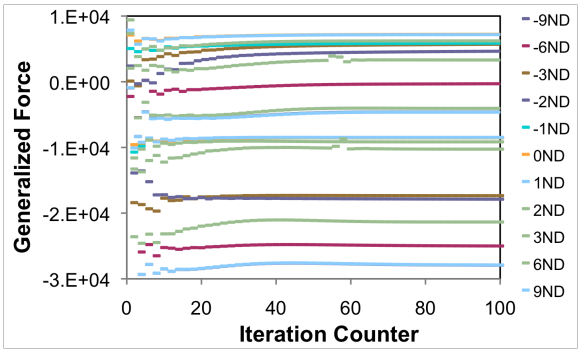


Figure 7.—HB unsteady solution convergence for first vibration mode.

## 3.2 Unsteady Computational Results

Unsteady computations were performed using the HB code to predict the aeroelastic stability of the fan. These computations were carried out at both 100 and 70 percent speeds for the first and second structural vibration modes (bending and torsion) and several nodal diameter (ND) patterns (see Eq. (4)). The blade mode shapes are shown in Figure 6 as un-scaled contour plots of modal displacements at 100 percent speed. The mode shapes at 70 percent speed are substantially similar to those at 100 percent speed. HB and TURBO unsteady computations were carried out at various steady conditions for both speeds, which enabled trends along the speed line to be assessed.

### 3.2.1 100 Percent Speed, First Vibration Mode

At 100 percent speed, computations were carried out for the first blade vibration mode and several ND of the travelling wave covering the entire possible range. Figure 7 shows the convergence of the unsteady HB computations as a plot of non-dimensional complex generalized force with iteration counter, for various values of nodal diameter (–9 to 9). These HB computations were for an operating point near stall with a non-dimensional back-pressure of 1.11. As can be noted, although the rates of convergence vary somewhat with nodal diameter, all the results are very well converged. Similar convergence characteristics were observed for other operating conditions or back-pressure values.

Figure 8 shows the variation of the converged generalized force with nodal diameter for vibration in the first mode at a back-pressure value of 1.11 at 100 percent speed. For a single vibration mode, the stability is determined by the imaginary part of the generalized force and Figure 8 shows that the imaginary part of generalized force is negative for all nodal diameters, indicating flutter stability. Also, nodal diameters near zero have the lowest stability.

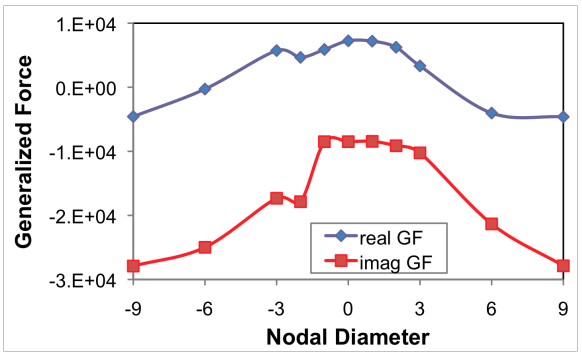


Figure 8.—HB generalized force variation with nodal diameter for 100 percent speed, back-pressure 1.11, first mode.

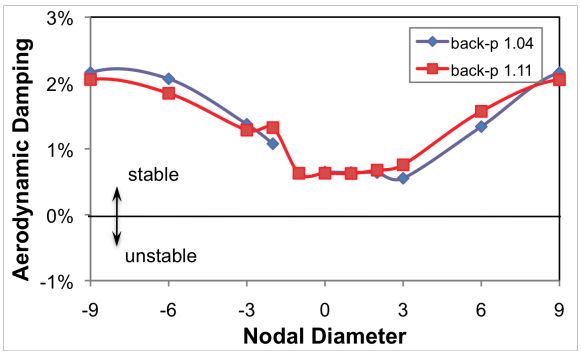


Figure 9.—Variation of HB aerodynamic damping with nodal diameter for 100 percent speed, first mode.

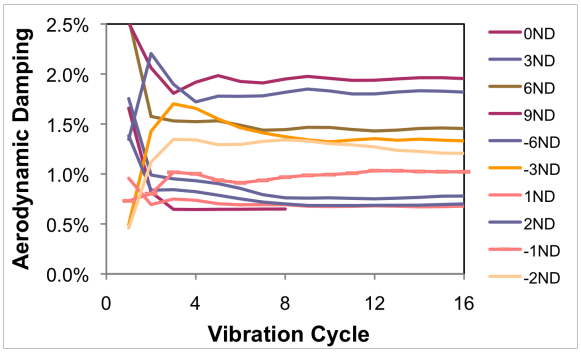


Figure 10.—TURBO unsteady solution convergence for first vibration mode.

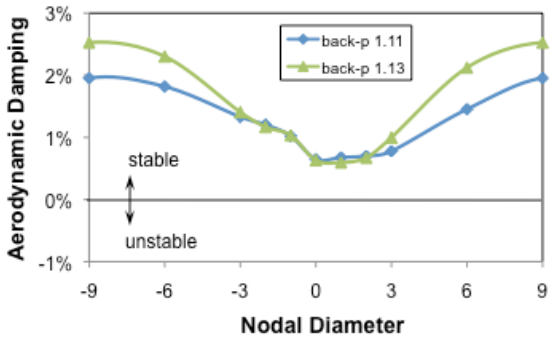


Figure 11.—Variation of TURBO aerodynamic damping with nodal diameter for 100 percent speed, first mode.

The generalized force values, shown in Figure 8, were used to calculate the aerodynamic damping, which is plotted in Figure 9. The results are presented for back-pressure values near of 1.11 (near stall) and 1.04 (away from stall). The aerodynamic damping, which is positive for all nodal diameters, is seen to vary by about 1.5 percent over the range, in contrast to previous results (Ref. 2) for a different configuration where the aerodynamic damping varied by an order of magnitude with nodal diameter. Also, for any given nodal diameter, the aerodynamic damping increases or decreases by only a small amount as back-pressure is changed, indicating only a weak dependence on operating condition. The lowest value of aerodynamic damping at a back-pressure of 1.11 is about 0.6 percent and occurs at 1ND.

For evaluating flutter stability at a fixed rotational speed, the trend in aerodynamic damping is relevant. Thus, in Figure 9, nodal diameters for which aerodynamic damping decreases with decreasing mass flow rate (increasing back-pressure) are particularly interesting. Nodal diameters of 3ND and 6ND are not of particular interest since the aerodynamic damping is increasing as we approach the stall line. Also, –3ND, –6ND, and ±9ND are not of particular interest because of the relatively large value of aerodynamic damping and relatively small variation with back-pressure. That leaves the low nodal diameters, which show low aerodynamic damping. But, they do not show much variation with back-pressure in this case.

The time-domain TURBO code was used for similar unsteady computations for 100 percent speed and first structural vibration mode. Figures 10 and 11 show the corresponding results. Figure 10 shows the convergence of the unsteady computations in the form of aerodynamic damping calculated at the end of each vibration cycle. For the various nodal diameters considered, the unsteady results are well converged. Figure 11 shows the variation of aerodynamic damping for various nodal diameters for two values of back-pressure: 1.11 and 1.13, which are both near the stall line. The lowest value of aerodynamic damping at a back-pressure of 1.13 is about 0.6 percent at 1ND. The range of variation with

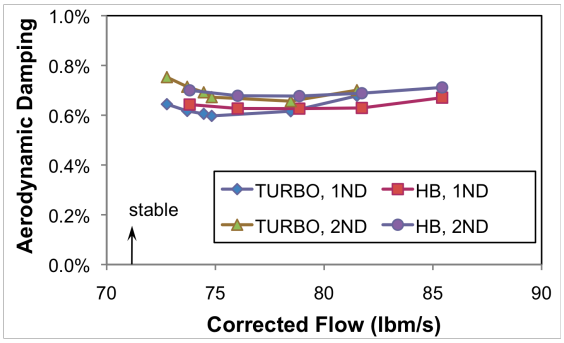


Figure 12.—Variation of aerodynamic damping with mass flow rate for 100 percent speed, first mode.

nodal diameter is about 2 percent. The trend with increasing back-pressure is one of increasing aerodynamic damping (more stable) for large nodal diameters >3 and <–3. For low nodal diameters, there is only a small variation with back-pressure, which is the same trend noted in the HB results.

The TURBO results in Figure 11 are very similar to the HB results in Figure 9. Recall that the operating points (mass flow rate) calculated from HB and TURBO are not the same for a given back-pressure, as shown in Figure 4. Hence, the aerodynamic damping from Figures 9 and 11 is not expected to match for the same values of back-pressure. Nonetheless, the observed trends are very similar. One notable difference is seen in the comparison of the trends at large positive and large negative nodal diameters. The TURBO results show the same trend, increasing stability with increasing back-pressure, at both positive and negative high nodal diameters. However, the HB results show a smaller variation with back-pressure and the trends for large positive nodal diameters are opposite to those for large negative nodal diameters.

Unsteady computations were performed at additional back-pressure values for 1ND and 2ND traveling wave patterns. The resulting variation of aerodynamic damping with mass flow rate, computed from both the HB and TURBO codes, is shown in Figure 12. The results correlate very well between the two analyses in terms of the calculated values of damping, the relative values of damping for the 1ND and 2ND traveling wave patterns, and the relatively small change with mass flow rate. The only notable difference is that the TURBO results show some weak trend with increasing and decreasing mass flow rate, whereas the HB results are largely unchanged for the mass flow rates considered. Based on the levels of aerodynamic damping calculated from HB and TURBO analyses, and the absence of any significant decrease along the speedline, no flutter is expected in the first mode at design speed.

### 3.2.2 100 Percent Speed, Second Vibration Mode

Unsteady computations were carried out for the second vibration mode in a manner similar to that described in the previous sub-section for the first vibration mode. Selected results are presented in this section. Figures 13 and 14 show the HB and TURBO variations of aerodynamic damping with nodal diameter for the two values of back-pressure used for the first mode calculations. A comparison between the two sets of results shows the similarities in the variation with nodal diameter. The amount of variation is significantly smaller than that obtained for the first mode. The lowest values of aerodynamic damping are smaller than those for the first mode. Also, Figures 13 and 14 show a similar trend with changing back-pressure. Results for 3ND and 6ND show significant variation with backpressure and a decrease with mass flow rate towards the stall line. Additional computations (with both HB and TURBO codes) are performed for these nodal diameter patterns and the results are presented in Figure 15 as variations of aerodynamic damping with mass flow rate. The results correlate very well between the two analyses in terms of the calculated values of damping and the relative values of damping for the 3ND and 6ND traveling wave patterns. Some difference is noted in terms of the slope of the variations with mass flow rate. The TURBO results show a clear linear trend, whereas the HB results show a smaller slope for 6ND and very little variation for 3ND.

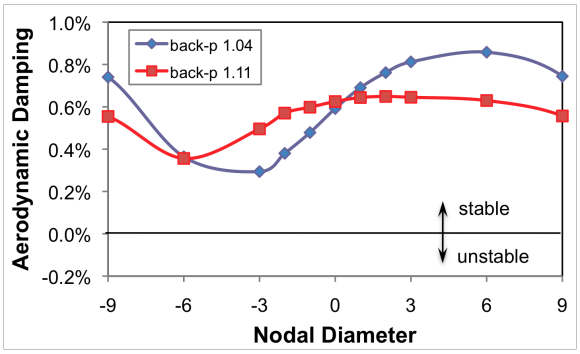


Figure 13.—Variation of HB aerodynamic damping with nodal diameter for 100 percent speed, second mode.

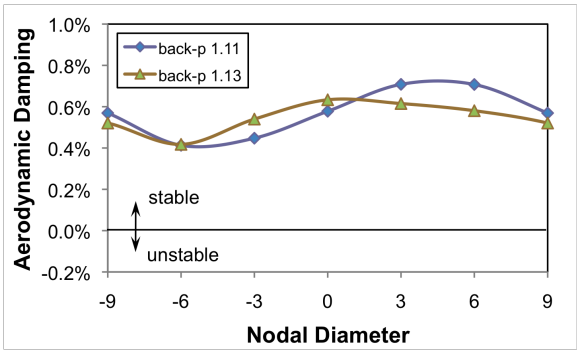


Figure 14.—Variation of TURBO aerodynamic damping with nodal diameter for 100 percent speed, second mode.

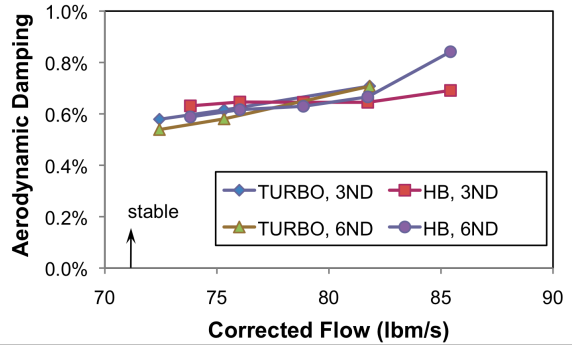


Figure 15.—Variation of aerodynamic damping with mass flow rate for 100 percent speed, second mode.

Since the aerodynamic damping drops slightly along the speedline, it is possible to extrapolate to a condition where the aerodynamic damping goes to zero. However, for the present configuration, it is clear that such calculated flutter points would fall considerably beyond the stall line (64 to 68 lbm/s depending on pressure ratio) shown in Figure 3. Thus, no flutter is expected in the second mode at design speed within the normal operating region. The computational results for 100 percent speed correlate well with the experimental observation of no flutter during wind-tunnel testing.

### 3.2.3 70 Percent Speed

Unsteady computations were carried out at 70 percent speed for the first and second vibration modes. The blade geometry and computational grids used were the same as those used for the 100 percent analyses. Selected results are presented here. Figure 16 shows the variation of HB aerodynamic damping with nodal diameter for the first vibration mode at 100 and 70 percent speeds. The same back-pressure value was prescribed for both sets of computations. The trend in variation with nodal diameter is essentially the same for both speeds; the lowest aerodynamic damping value changes from 0.6 percent at 100 percent speed to 0.4 percent at 70 percent speed. Figure 17 shows the corresponding results for the second vibration mode, for which some change in the variation with nodal diameter is noted, with a peak occurring near –3ND for 70 percent speed.

Figure 18 shows the variation of aerodynamic damping with back-pressure for the second mode. In terms of the variation along the speedline (with back-pressure), the notable trend is the large drop at 6ND and 9ND when back-pressure is increased from 1.04 to 1.11. Based on the low aerodynamic damping at 9ND, additional computations were done for this nodal diameter at 70 percent speed. The results are presented in Figure 19. Both the HB and TURBO show very similar values and trends, with a notable difference in the slope.

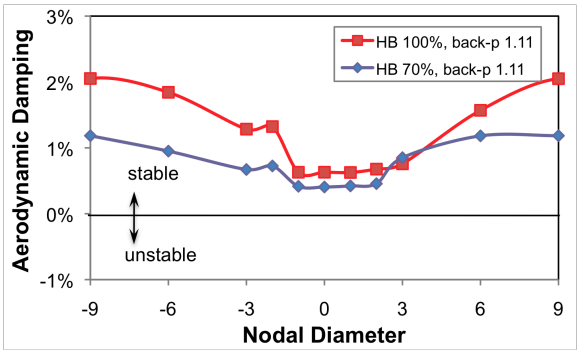


Figure 16.—Variation of HB aerodynamic damping with nodal diameter at 100 and 70 percent speeds, first mode.

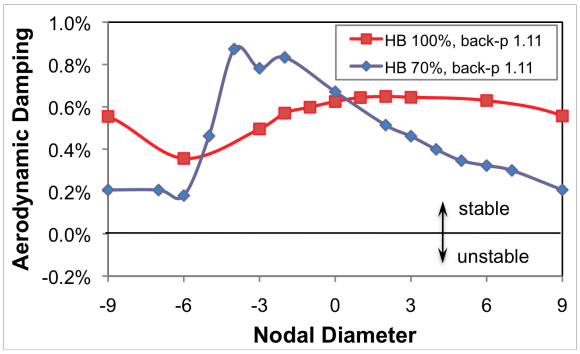


Figure 17.—Variation of HB aerodynamic damping with nodal diameter at 100 and 70 percent speeds, second mode.

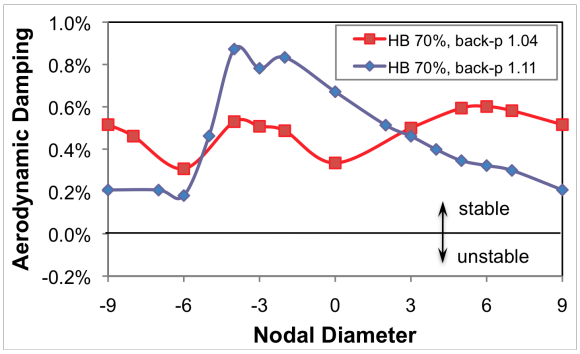


Figure 18.—Variation of HB aerodynamic damping with nodal diameter and back-pressure; 70 percent speed, second mode.

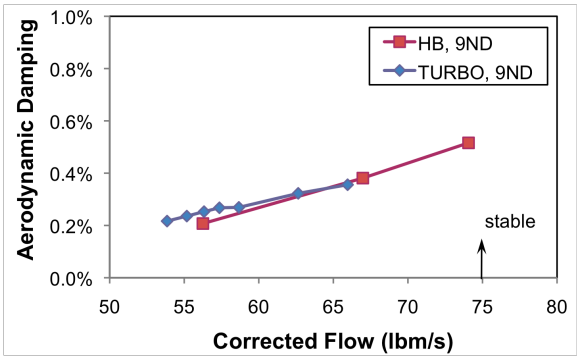


Figure 19.—Variation of aerodynamic damping with mass flow rate for 70 percent speed; second mode, 9ND pattern.

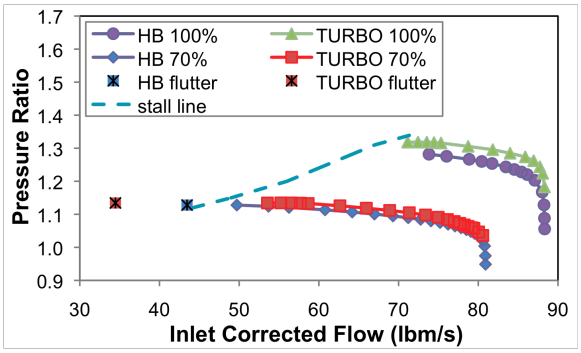


Figure 20.—Fan map showing flutter points.

Based on the nearly linear variation, it is possible to extrapolate to zero aerodynamic damping; the mass flow rate at the calculated flutter point is approximately 44.4 lbm/s based on HB results, and approximately 34.5 lbm/s based on TURBO results. Notably, both these fall beyond the stall line (46 to 47 lbm/s depending on pressure ratio), although the TURBO results indicate a far larger margin than indicated by the HB results, as shown in Figure 20. Note that this trend in flutter results from the two analysis codes is consistent with previous part-speed results for another fan configuration as reported in (Ref. 7), namely, that the HB result points to a flutter point at a higher mass flow rate as compared to TURBO. Further work is needed to understand the differences in the rate of change of aerodynamic damping along the speedline from the two analyses. Note that both results are consistent with the observation of no flutter during wind-tunnel testing.

# 4.0 Conclusions

Steady and unsteady computations have been carried out for an experimental fan configuration using two turbomachinery aeroelastic analysis codes that solve the RANS equations with blade vibrations using a time-marching method (TURBO) and a HB. The computational results were summarized and compared. Overall, the TURBO and HB results are in good agreement. The steady results were compared on the performance map and correlate well. The steady HB results show a slightly lower pressure ratio than the steady TURBO results for the same mass flow rate, which is consistent with previous results for a different configuration. The difference in calculated pressure ratio is higher for the design speed than for the selected part-speed. For the same imposed back-pressure, the HB computations resulted in lower mass flow rates. The variation of efficiency with mass flow rate was compared and found to agree well with small difference near stall (HB calculations yield slightly higher values near stall). A detailed look at the flowfields predicted by HB and TURBO may provide additional information regarding the source of these differences.

Unsteady computations have been performed at design speed for the first two structural vibration modes for various nodal diameter patterns. Both HB and TURBO computational results show very similar levels and trends of aerodynamic damping variations with nodal diameter. The range of variation with nodal diameter is less than 2 percent, in contrast to results previously obtained for a different fan. The second mode is seen to have a slightly lower aerodynamic damping than the first mode. The variations of aerodynamic damping with mass flow rate (along a speedline) are examined for the least stable nodal diameter patterns. The levels and trends correlate quite well between the two analyses. For the first vibration mode, both analyses show no significant decrease in aerodynamic damping along the speedline, leading to the conclusion that no flutter is expected, which correlates with the experimental observation of flutter stability. For the second mode, both analyses show that the aerodynamic damping for the +6ND nodal diameter pattern decreases slowly towards stall. However, with an aerodynamic damping value more than 0.5 percent, no flutter is expected. The computational results correlate well with the experimental observation of no flutter during wind-tunnel testing.

For 70 percent speed, the results for the first vibration mode are similar to those for 100 percent speed except for lower levels of aerodynamic damping. For the second mode, the 9ND nodal diameter pattern is seen to have a low level of aerodynamic damping along with a large rate of decrease in it towards the stall line. Based on the TURBO results, the extrapolated flutter point is well beyond the stall line, indicating no flutter in the normal operating region. The HB results also show that the extrapolated flutter point is beyond the stall line but very close to it in contrast to the TURBO results. Note that these results are consistent with the observation of no flutter during wind-tunnel testing. Further work is needed to understand the differences in the rate of change of aerodynamic damping along the speedline calculated by the two analyses, which resulted in different extrapolated flutter points.

In the present study, very small amplitude vibrations were prescribed to calculate linearized unsteady aerodynamics for a conventional linear flutter analysis as a first step to understand the characteristics of the HB code and of the flutter of an experimental fan. Future work will investigate the non-linear amplitude-dependent effects using the same HB aeroelastic code and the time-domain TURBO codes.

# References


1. Marshall, J.G., and M. Imregun, "A review of aeroelasticity methods with emphasis on turbomachinery applications," *Journal of Fluids and Structures*, Vol. 10, 1996, pp. 237–267.
2. Bakhle, M.A., Srivastava, R., Panovsky, J., Keith, T.G., Jr., Stefko, G.L., "Flutter Calculations of an Experimental Fan," Paper US-2, CEAS/AIAA/NVvL International Forum on Aeroelasticity and Structural Dynamics, Amsterdam, June 4–6, 2003.
3. Srivastava, R., Bakhle, M.A., and Keith, T.G., Jr., "Numerical Simulation of Aerodynamic Damping for Flutter Analysis of Turbomachinery Blade Rows," *Journal of Propulsion and Power*, Vol. 19, No. 2, March–April 2003.

4. Hall, K.C., Thomas, J.P., and Clark, W.S., "Computation of Unsteady Nonlinear Flows in Cascades Using a Harmonic Balance Technique," *AIAA Journal*, Vol. 40, No. 5, May 2002.
5. Ekici, K., Hall, K.C., "Nonlinear Analysis of Unsteady Flows in Multistage Turbomachines Using Harmonic Balance," *AIAA Journal*, Vol. 45, No. 5, May 2007, pp. 1047–1057.
6. Fite, E.B., Woodward, R.P., and Podboy, G.G., "Effect of Trailing Edge Flow Injection on Fan Noise and Aerodynamic Performance," AIAA Paper 2006–2844, June 2006.
7. Bakhle, M.A., Thomas, J.P., and Reddy, T.S.R., "Fan Flutter Computations Using the Harmonic Balance Method," AIAA Paper 2008–4743, July 2008.
8. Carta, F.O., "Coupled Blade-Disk-Shroud Flutter Instabilities in Turbojet Engine Rotors," *Journal of Engineering for Power*, July 1967, pp. 419–426.

| REPORT DOCUMENTATION PAGE | | | Form Approved OMB No. 0704-0188 |
|---|---|---|---|



| 1. REPORT DATE *(DD-MM-YYYY)* | 2. REPORT TYPE | 3. DATES COVERED *(From - To)* |
|---|---|---|
| 01-08-2010 | Technical Memorandum | |

**4. TITLE AND SUBTITLE**
Harmonic Balance Computations of Fan Aeroelastic Stability

**5a. CONTRACT NUMBER**

**5b. GRANT NUMBER**

**5c. PROGRAM ELEMENT NUMBER**

**6. AUTHOR(S)**
Bakhle, Milind, A.; Reddy, T.S.R.

**5d. PROJECT NUMBER**

**5e. TASK NUMBER**

**5f. WORK UNIT NUMBER**
WBS 561581.02.08.03.21.03

**7. PERFORMING ORGANIZATION NAME(S) AND ADDRESS(ES)**
National Aeronautics and Space Administration
John H. Glenn Research Center at Lewis Field
Cleveland, Ohio 44135-3191

**8. PERFORMING ORGANIZATION REPORT NUMBER**
E-17203

**9. SPONSORING/MONITORING AGENCY NAME(S) AND ADDRESS(ES)**
National Aeronautics and Space Administration
Washington, DC 20546-0001

**10. SPONSORING/MONITOR'S ACRONYM(S)**
NASA

**11. SPONSORING/MONITORING REPORT NUMBER**
NASA/TM-2010-216222

**12. DISTRIBUTION/AVAILABILITY STATEMENT**
Unclassified-Unlimited
Subject Categories: 07 and 05
Available electronically at http://gltrs.grc.nasa.gov
This publication is available from the NASA Center for AeroSpace Information, 443-757-5802

**13. SUPPLEMENTARY NOTES**

**14. ABSTRACT**
A harmonic balance (HB) aeroelastic analysis, which has been recently developed, was used to determine the aeroelastic stability (flutter) characteristics of an experimental fan. To assess the numerical accuracy of this HB aeroelastic analysis, a time-domain aeroelastic analysis was also used to determine the aeroelastic stability characteristics of the same fan. Both of these three-dimensional analysis codes model the unsteady flowfield due to blade vibrations using the Reynolds-averaged Navier-Stokes (RANS) equations. In the HB analysis, the unsteady flow equations are converted to a HB form and solved using a pseudo-time marching method. In the time-domain analysis, the unsteady flow equations are solved using an implicit time-marching approach. Steady and unsteady computations for two vibration modes were carried out at two rotational speeds: 100 percent (design) and 70 percent (part-speed). The steady and unsteady results obtained from the two analysis methods compare well, thus verifying the recently developed HB aeroelastic analysis. Based on the results, the experimental fan was found to have no aeroelastic instability (flutter) at the conditions examined in this study.

**15. SUBJECT TERMS**
Fan blades; Flutter; Reynolds-averaged Navier-Stokes equation; Turbomachinery; Aeroelasticity; Aeroelastic stability

| 16. SECURITY CLASSIFICATION OF: | | | 17. LIMITATION OF ABSTRACT | 18. NUMBER OF PAGES | 19a. NAME OF RESPONSIBLE PERSON |
|---|---|---|---|---|---|
| a. REPORT | b. ABSTRACT | c. THIS PAGE | | | STI Help Desk (email:help@sti.nasa.gov) |
| U | U | U | UU | 19 | 19b. TELEPHONE NUMBER *(include area code)* 443-757-5802 |